Steel and Composite Structures, *Vol. 38, No. 4 (2021) 365-380*
DOI: https://doi.org/10.12989/scs.2021.38.4.365

Static behavior of bolt connected steel-concrete composite beam without post-cast zone

Ying Xing[1,2], Yun Zhao[1], Qi Guo*[1], Jin-feng Jiao[1], Qing-wei Chen[3] and Ben-zhao Fu[4]

[1]College of Civil Engineering, Taiyuan University of Technology, Taiyuan 030024, China
[2]College of Civil Engineering, Hunan University, Changsha 410082, China
[3]Economic & Technology Research Institute of State Grid Shandong Electric Power Company, Jinan 250021, China
[4]State GRID Fujian Economic Research Institute, Fuzhou 350000, China

(*Received October 26, 2020, Revised January 7, 2021, Accepted January 29, 2021*)

Abstract. Although traditional steel-concrete composite beams have excellent structural characteristics, it cannot meet the requirement of quick assembly and repair in the engineering. This paper presents a study on static behavior of bolt connected steel-concrete composite beam without post-cast zone. A three-dimensional finite element model was developed with its accuracy and reliability validated by available experimental results. The analysis results show that in the normal service stage, the bolt is basically in the state of unidirectional stress with the loss of pretightening can be ignored. Parametric studies are presented to quantify the effects of the post-cast zone, size and position of splicing gap on the behavior of the beam. Based on the studies, suggested size of gap and installation order were proposed. It is also confirmed that optimized concrete slab in mid-span can reduce the requirement of construction accuracy.

Keywords: high-strength frictional bolt; steel-concrete composite beam; post-cast zone; prefabricated construction

1. Introduction

As a result of the benefits of combining the advantages of its components, steel–concrete composite beams have been widely used and studied. Nie (2009) conducted some tests of composite beam under combined bending and torsion, founding that the reinforced concrete slab contributes mainly to the torsional resistance of composite beams. Han (2015) concluded that the strength for the composite beam with large stud can be increased by recycled tire rubber-filled concrete, and the quantity and width of cracks can be reduced efficiently. Liu (2016) performed parametric analysis on shear connection degree, diameter of stud, stud arrangement, beam length, and loading way through experimental and finite element modeling. Furthermore, Sheehan (2018) concluded that with low degree of shear connection, the maximum bending moment of the composite beam was close to the plastic bending resistance according to the Eurocode 4. Wang (2019) conducted the push-out tests with cast-in-place concrete decks and precast concrete decks. It was concluded that shear resistance was observed significant reduction when tension was applied. Besides, Fan (2020) proposed that the stiffness and crack resistance of the steel engineered cementitious composite (ECC) composite beams was enhanced significantly under negative bending moments.

However, the headed studs, which welded to the steel beam and embedded in the casting concrete, are usually fatigue fractured under traffic loads. What's more, it is hard to separate the steel beam from concrete plate, and weld a new stud without concrete broken. Therefore, the repeated casting of concrete will cause not only environmental pollution but also resource waste. In recent years, as the demand of structural design is changing from damage preventing to maintainable and restorable structural functions, a new composite beam with prefabricated concrete slab, steel beam and high-strength frictional bolt was proposed. For this promising composite beam, the failed bolts can be unbolted and replaced easily without concrete broken, and it is convenient for assembling.

The bolts were firstly applied into composite beam as shear connectors in the 1960s.They were embedded in the concrete slab and post-tensioned after the casting concrete reached its strength (Dallam 1968). In the 1970s, after drilling holes on assembled concrete slab and steel beam, bolts was used to connect them, and the composite action was corroborated (Marshall 1971). Recently, a few tests have been conducted to obtain the mechanical property of the assembled bolt connected composite beams. Kwon (2010) conducted static and fatigue tests on composite beams with three different connecting method of bolts. It was found that bolt connected composite beams had a better fatigue behavior than studs connected ones. In addition, its feasibility of the application in bridge strengthening was verified. Pavlović (2013) elucidated the good bearing capacity of the single embedded bolt, but pointed out its poor shear stiffness. Then, Dai (2015) and Rehman (2016) concluded demountable shear connectors can be easily demounted after testing and have similar capacity and behavior to welded shear connectors. Also, Ataei (2016)

∗Corresponding author, Senior Engineer
E-mail: guoqi_tony@163.com

http://www.techno-press.org/?journal=scs&subpage=8
ISSN: 1229-9367 (Print), 1598-6233 (Online)

realized that bolt connected composite beams can enhance its plasticity and ductility, on the condition of the same shear stiffness. In addition, it was manifest that all the concrete slabs, steel beam and bolts can be reused. Pathirana (2016) conducted the composite beam tests with two blind bolt types and welded stud connectors， which proving the comparable ability of the blind bolts of the welded stud connectors. Afterwards, Liu (2017) performed parametric analysis on bolt connected composite beams. The influences of hole number and diameter, type of concrete, and steel grade of joist on mechanical properties were investigated, and the calculating method of ultimate flexural strength was proposed. Balkos (2019) conducted the static and fatigue tests of three beam specimens with through-bolt shear connectors, concluding that the fatigue performance of the through-bolt shear connectors far exceeded that of welded shear studs. Moreover, some studies suggested that the shear bearing capacity of the bolted connector mainly depended on the bolt diameter, the bolt tensile strength and the concrete strength (Zhang 2019), and the specimens with small bolt hole achieve significantly higher pre-slip and post-slip shear stiffness compared to specimens with large bolt hole diameter (Zhao 2020). Yang (2020) concluded the average ultimate shear resistance per bolt for the push-out specimens with two and three rows of bolt shear connectors was reduced comparing with the push-out specimen possessing single-row bolts. Recently, Ataei (2021) proposed the deconstrcutable steel-concrete composite bolted shear connectors have completely different behaviour compared to welded headed stud shear connectors through push-out tests.

Generally, the high-strength frictional bolt connected composite beam was proved available (Chen 2014). Furthermore, the friction-based shear connector promotes accelerated bridge construction by fully exploiting prefabrication and allows rapid bridge disassembly to drastically reduce the time needed to replace any deteriorating structural component (Suwaed 2018). However, most of the concrete slabs were pre-casted in the workshop and connected with post-cast zones at the construction site. Otherwise, concrete slabs should be drilled into holes after casting. Both methods increase the difficulty of disassembly, reuse and construction.

In this paper, a method of precast concrete slabs without post-cast zones was proposed. After verifying finite element model through tests data, the bolt mechanical property and its combination effects were studied. The influence of absence of post-cast zones was proposed. Besides, parametric analysis was carried out on the size and position of splicing gap. By adjusting the proper size of concrete slabs, an acceptable mechanical property was obtained with its behavior similar as the post-cast composite beam.

2. Numerical model

The composite beam tests conducted by Ataei (2016) was numerically simulated by ABAQUS software in this study. M20 frictional high-strength bolts were used as shear connectors in the test to realize the field assembly of concrete slabs and steel beams. What's more, the concrete slabs were segmented precast with no post-cast zone during assembly. The slabs was made of Geopolymer concrete with size of 1000×1000×150 mm, and the cross-section of the steel beam was 453.8×190×8.5×12.7 mm. The bolt pretightening force was 145kN. In order to ensure the correct installation of bolts, enlarged holes were adopted on the steel beams and concrete slabs. For model CB1, four bolts were used in each concrete slab, while only two bolts were used in each slab of CB2 except for end slabs. Composite beams were loaded at their four equal points. The details of CB1 and CB2 are shown in Fig. 1.

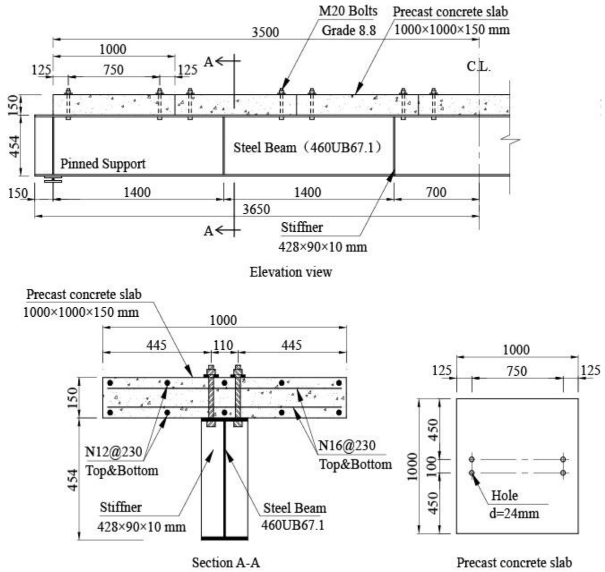

(a) CB1

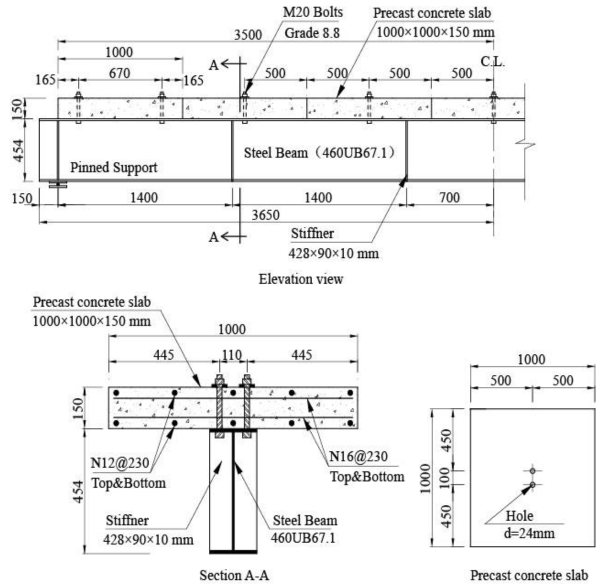

(b) CB2

Fig. 1 Details of the test models

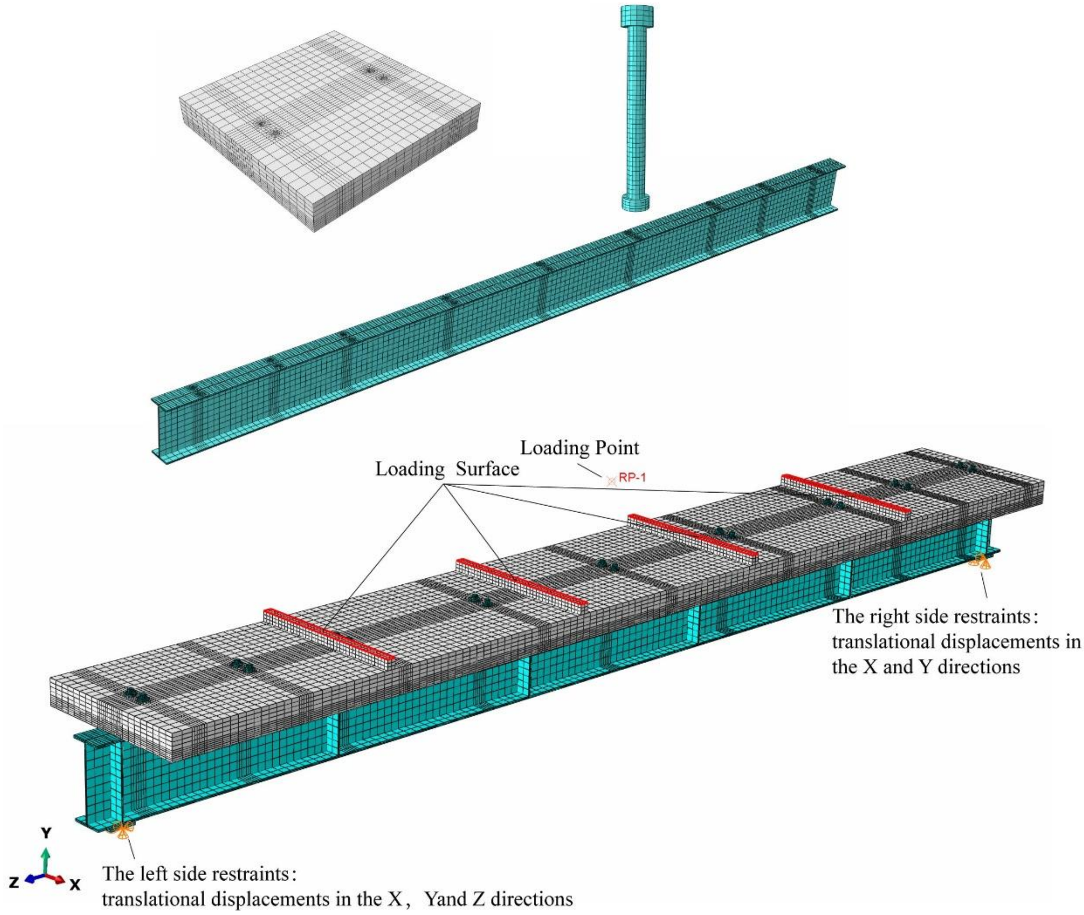

Fig. 2 Numerical model of composite beams

2.1 Element and mesh

For the concrete slab, steel beam and shear connector, a three-dimensional eight node element (C3D8R) with a linear approximation of displacement, reduced integration with hourglass control, eight nodes and three translational degrees of freedom was used. For the steel reinforcement, a three-dimensional truss element (T3D2) with a linear approximation of displacement, two nodes and three translational degrees of freedom was adopted. The overall mesh scale of concrete slabs and steel beams was 50 mm, while the smallest mesh scale of bolt holes and bolt connector was refined as 5 mm and 6 mm, respectively (shown in Fig. 2).

2.2 Interaction and boundary conditions

Once all components of the model were properly positioned together into the assembly, appropriate interaction and constraint conditions were defined among the various components. There are contact constraints such as steel beam-concrete slab, bolt-concrete slab and concrete slab-concrete slab during assembly, as shown in Fig. 3. The surface-to-surface contact interaction available in ABAQUS was applied at all the interfaces, in which HARD contact and PENALTY contact were used in normal direction and tangential direction, respectively. The friction coefficients were set as 0.45 for normal steel–concrete interfaces. As the influence of friction coefficients between concrete-concrete interface was proved to be inconsequential, it was valued as 0.8 according to Liu (2017), while the friction coefficient was set as 0.3 for all the other interactions. The embedded constraint was applied between the reinforcement and the concrete slab with the slip and bond ignored. (shown in Fig. 3)

The mechanical behavior of simply supported beams was mainly studied in this study. As a result, translational degrees of freedom in all 3 directions were constrained at left end, while X and Z directions were constrained at right end, as shown in Fig. 2.

2.3 Loading and analysis step

Implicit static analysis available in ABAQUS was adopted for numerical analysis, and all the analysis progress was divided into two steps. In the first step, the pretightening forces were applied to the bolts by using the orthotropic BOLT LOAD option. In the second step, the vertical loads were imposed as a displacement on the four loading points of composite beam, as shown in Fig. 2. At the same time, the bolts were set to fix at current length in this step to simulate the continuous pretightening force.

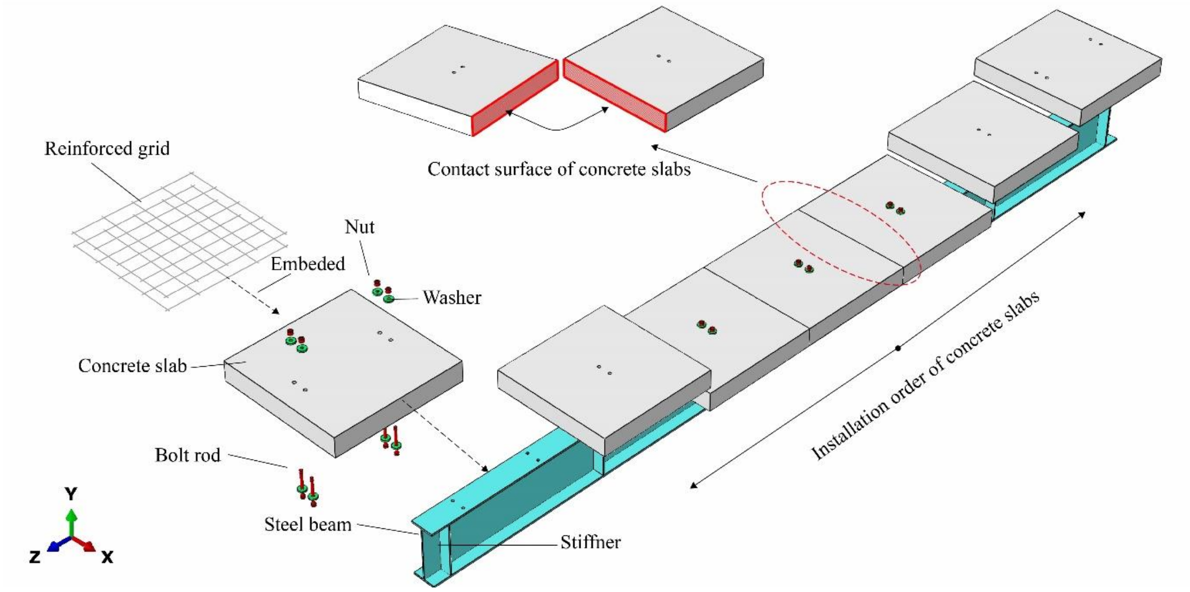

Fig. 3 Assembly of composite beam

2.4 Material properties

2.4.1 Geopolymer concrete

Plastic damage model was used in this study to simulate the crack behavior of concrete, in which the yield function proposed by Lee and Fenves (1998) was adopted. Angle of material expansion ψ, eccentricity e and material viscosity coefficient μ were set as 38° and 0.1 and 0.00001, respectively. Moreover, the ratio of biaxial compressive strength to uniaxial compressive strength σ_{b0}/σ_{c0} was 1.16, and the ratio of the second stress invariants on the tension and compression meridians K was 0.667.

According to the theory proposed by Hardjito (2005), the ralationship of stress and strain of geopolymer concrete can be described as Eq. (1), where f_c' is peak stress; ε_{co} is the peak strain corresponding to the peak stress valued as 0.0036; limiting strain ε_{cu} is 0.01. The concrete around bolt hole was in a triaxial stress state, which might improve the compressive capacity of concrete. As a result, the descending part of the stress-strain curve was simplified as horizontal line in the Fig. 4(a). The elasticity modulus was calculated as Eq. (3), and the poisson ratio was 0.14.

$$\sigma_c = f_c' \frac{\varepsilon_c}{\varepsilon_{co}} \frac{n}{n-1+(\varepsilon_c/\varepsilon_{co})^{nk}};\ \ n = 0.8 + \frac{f_c'}{12} \tag{1}$$

$$k = \begin{cases} 0.67 + (f_c'/62) & \varepsilon_c/\varepsilon_{co} > 1 \\ 1 & \varepsilon_c/\varepsilon_{co} \le 1 \end{cases} \tag{2}$$

$$E_c = 5300 + 2707\sqrt{f_c'} \tag{3}$$

The relationship between the tensile capacity and compressive capacity of geopolymer concrete is shown in Eq. (4). The stress-strain relationship in Fig. 4(c) was assumed to be linear before and after cracking. The geopolymer concrete was adopted in model validation in section 3.

$$f_{t,sp} = 0.7\sqrt{f_c'} \tag{4}$$

2.4.2 Common concrete

The compressive stress-strain curve of common concrete, based on Hognestad's model, can be simplified into three parts. The elastic stage and nonlinear stage were calculated according to Eqs. (5) and (6), where f_c' is 0.85 times of compressive ultimate strength; ε_{co} is the peak strain valued as 0.002; ε_{cu} is the ultimate strain valued as 0.01. The descent stage was simplified as line considering the triaxial stress state, as shown in Fig. 4(b).

$$\begin{cases} \sigma_c = E_c\varepsilon_c & \sigma_c \le 0.45f_c' \\ \sigma_c = f_c'\left[\frac{2\varepsilon_c}{\varepsilon_{co}} - \left(\frac{\varepsilon_c}{\varepsilon_{co}}\right)^2\right] & 0.45f_c' \le \sigma_c \le f_c' \end{cases} \tag{5}$$

$$E_c = 12.4 \times 10^3 + 460f_c' \tag{6}$$

The tensile ultimate strength of common concrete was 0.1 times the compressive ultimate strength, and the tensile stress-strain curve was simplified as geopolymer concrete. The common concrete was adopted in mechanism analysis and parametric analysis in section 4 and section 5, respectively.

2.4.3 Steel beams, bolts and reinforcement

The elastic-plastic model combining Prandtl-Reuess plastic flow criterion and isotropic strain hardening was used to describe the properties of steel beams, as shown in Fig. 5(a). In the figure, $E_s = 200GPa$, $\varepsilon_{st} = 0.02$, $\varepsilon_{su} = 0.25$, Poisson's ratio is 0.3.

The three-fold line constitutive relation proposed by Lon (2006) was adopted for bolts, as shown in Fig. 5(b), where f_{btu} is the ultimate bearing capacity of bolts, and the yield stress is $0.94f_{btu}$; ε_{bty} is the yield strain, and the ultimate strain is $8\varepsilon_{bty}$; the fracture strain of bolt is 0.15(Shi 2008).

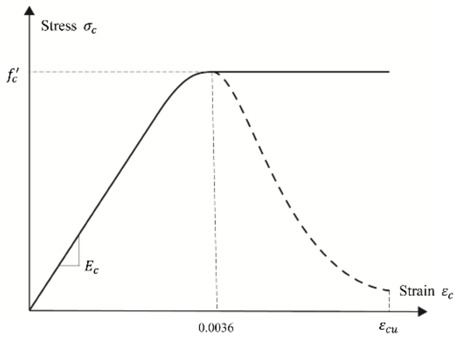

(a) Compressive geopolymer concrete

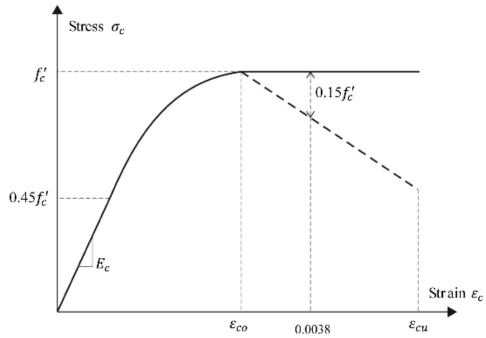

(b) Compressive common concrete

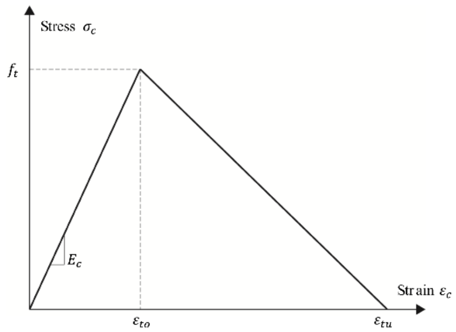

(c) tensile concrete

Fig. 4 Stress-strain curves of concrete

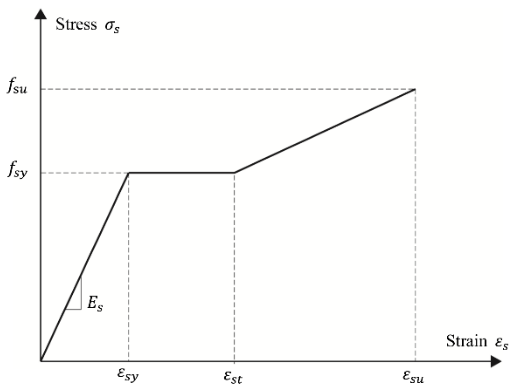

(a) Steel beam

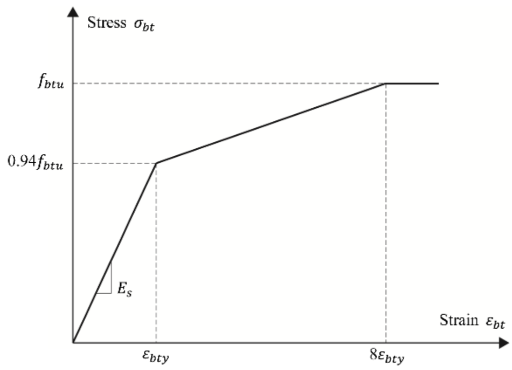

(b) High strength frictional bolts

Fig. 5 Stress-strain curves of Steel material

Table 1 Properties of steel materials

Specimen	yield strength (MPa)	Ultimate strength (MPa)	Young's modulus (GPa)
Steel beam flange (Liu 2017)	351.2	533.3	200
Steel beam web (Liu 2017)	406.1	551.4	205
Bolt connector (Ataei 2016)	936	969	210
Steel bar (Ataei 2016)	543	640	200

Table 2 Properties of concrete materials (Ataei 2016)

Specimen	Compressive strength (MPa)	Tensile strength (MPa)	Young's modulus (GPa)
CB1	40.9	4.3	21.1
CB2	39.7	4.7	NA

Ideal elastic-plastic model was adopted in the stress-strain curve of reinforcement considering no strain hardening. The material strength is shown in Tables 1 and 2.

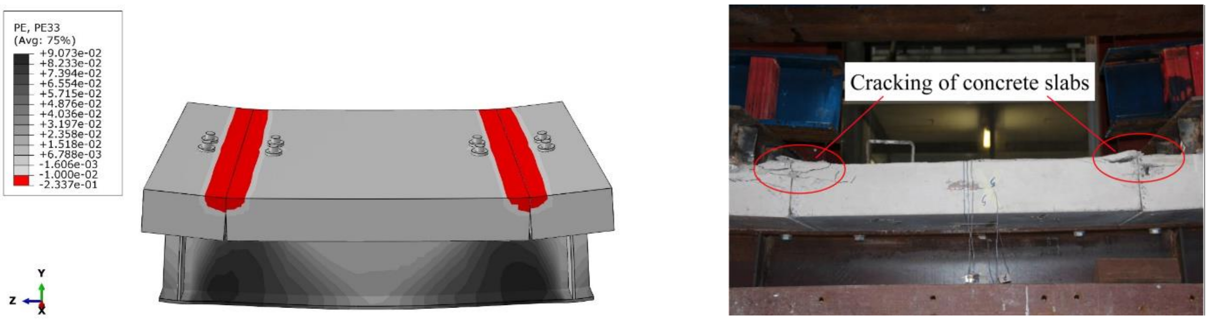

(a) Finite element (b) Test

Fig. 6 Crack of mid-span concrete slab in CB1

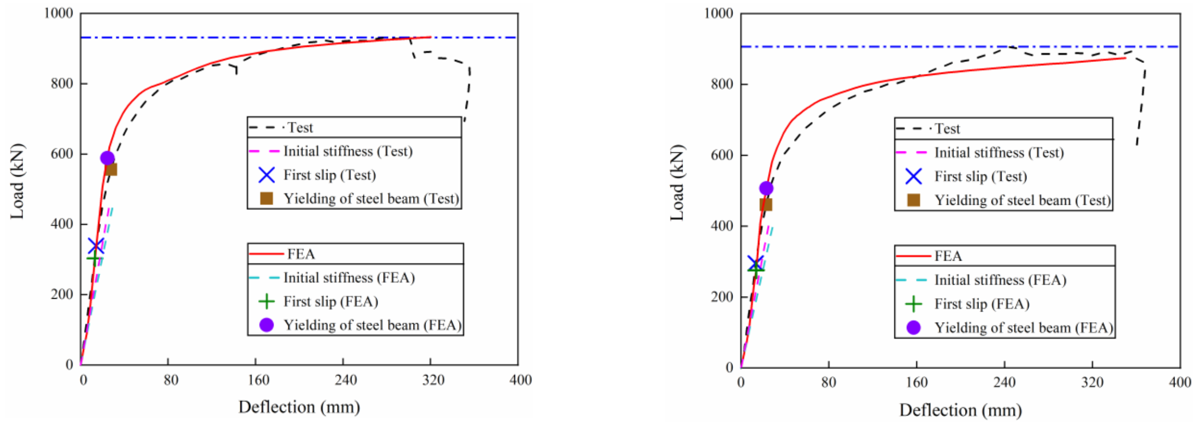

(a) CB1 (b) CB2

Fig. 7 Load-deflection curves of FEA and test results

3. Model validation and analysis

The failure mode obtained from test and finite element analysis (FEA) were demonstrated in Fig. 6. It can be seen from the figure that concrete slab cracked at the top of mid-span, while concrete slabs naturally separated at bottom due to the absence of post-cast trip. The finite element results were in good agreement with the experimental results.

Fig. 7 shows the load-deflection curves obtained from the test and FEA. The predicted initial stiffness for CB1 and CB2 were 12.8% and 10.1% lower than the test values respectively. The ultimate load obtained from the FEA were 0.1% and 6.53% less than the experimental value respectively, from which it can be seen that the two results are in good agreement.

The FEA and experimental results for the relationship between load and relative longitudinal slip at the support end were shown in Fig. 8. FEA shown that when the load reached 304 kN and 279 kN, the friction force of interface at the end of support was overcame for CB1 and CB2, respectively. These values were 10.59% and 12% less than the test values. In addition, the ultimate slip of CB1 and CB2 from FEA were 12.3% and 16.4% higher than the test values respectively. These differences might be attributed to the eccentric, asymmetry and size error of test specimens during the prefabrication and installation. Therefore, it was shown that the numerical model can predicted various behaviors of the composite beams.

4. Mechanism analysis of bolt and steel-concrete interface

The increasing relative longitudinal slip caused by continuous bending deformation lead to the overcoming of interface friction.

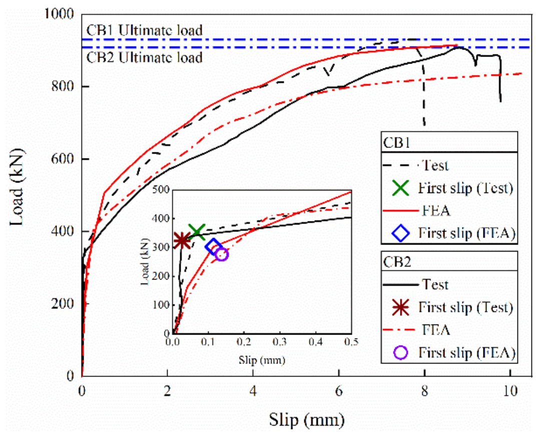

Fig. 8 Load-slip curves of support end

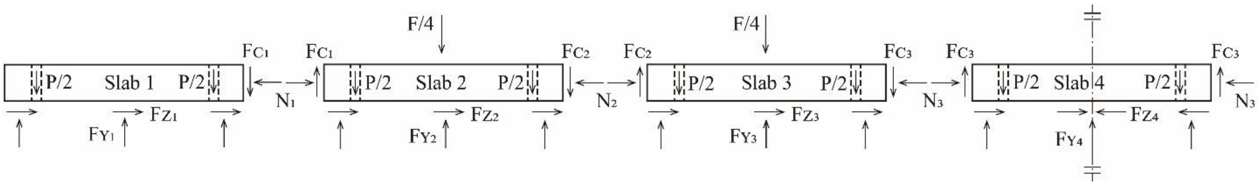

Fig. 9 Force transferring of interface and concrete slab

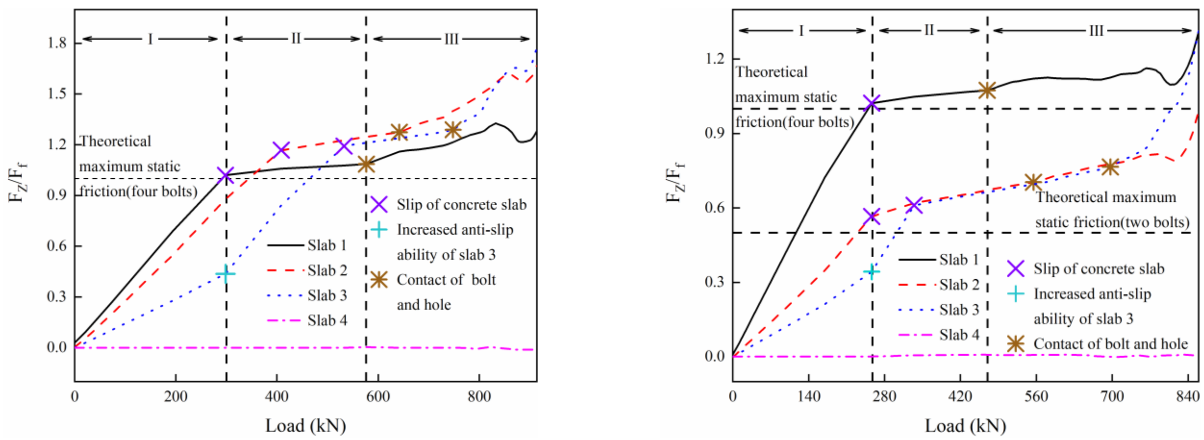

(a) CB1 (b) CB2

Fig. 10 F_Z/F_f-load curves

As a result, the bolt shear connector was in a complex stress state after connecting with bolt hole. However, the stress of bolt and interface cannot be obtained immediately from test. Therefore, normal compressive force(F_Y) and tangential shear force(F_Z) of steel-concrete interface obtained from FEM were analyzed. Moreover, the axial force, shear force and bending moment of the end bolt were described.

4.1 Steel-concrete interface

Common concrete with the compressive stress of 40MPa was used in the FEM of CB1 and CB2 instead of geopolymer concrete. Force transferring on interface and concrete slab was demonstrated in Fig. 9.

In the Fig. 9, F/4 was the external load and P was the total pretightening force of one single concrete slab. N_i and F_{Ci} were the axial force and friction force between concrete slabs, respectively. F_{Zi} and F_{Yi} were the total shear force and extrusion force on the interface between steel beam and concrete slab. As for slab 2 and slab 3, F_Y could be calculated as Eq. (7). When the interface friction has not been overcome, N_i could be calculated as Eq. (8). Therefore, $N_3 > N_2 > N_1$.

$$F_Y = F/4 + P \tag{7}$$

$$N_i = N_{i-1} + F_{Zi} \quad (i = 2, 3) \tag{8}$$

For model CB1 and CB2, the relationships between tangential friction and load were revealed in Fig.10, where F_f was total static friction force provided by 4 bolts in single slab.

It can be seen from the figure that the shear resistance of bolts can be divided into three stages. Stage I is fully friction stage, in which all the longitudinal shear force between the bottom surface of the concrete slab and the top steel flange was resisted by interface friction. As Slab 1 was located at the end of the composite beam, the shear force undertaken by Slab 1 was the largest, and that undertaken by Slab 3 was the smallest. Stage II is partial friction stage. In this stage, longitudinal slip of Slab 1 occurred after its shear force F_{Z1} exceeded maximum static friction force. However, the bolt in Slab 1 had not contacted the hole yet because the slip was not large enough. As a result, the shear force undertaken by Slab 1 would not increase furthermore, while the added shear force continued to be undertaken by Slab 2 and Slab 3. With the continuous increase of longitudinal shear force between interfaces, the maximum static friction force of Slab 2 and Slab 3 would be overcame in turn, resulting in their longitudinal relative slip in the same order. Stage III is fully pressure stage, in which friction forces of all the concrete slabs were overcame, and the longitudinal relative slip of composite beam grew rapidly. As a result, bolt shanks in Slab 1 firstly contacted the holes and then turned into pressure type bolts. In this way, could the shear force of composite beams continue to increase. In this stage, the bolts shanks in Slab 1, 2, and 3 switch into pressure type bolts in turn until the final failure of composite beam.

For the model CB1, the slip of Slab 1, 2, and 3 occurred at the loads of 300 kN, 410 kN and 533 kN respectively, and the bolts contacted with the holes at the loads of 576 kN, 641 kN and 748 kN, respectively. For the model CB2, as the bolts in Slab 2 were less than those in Slab 1, slip occurred

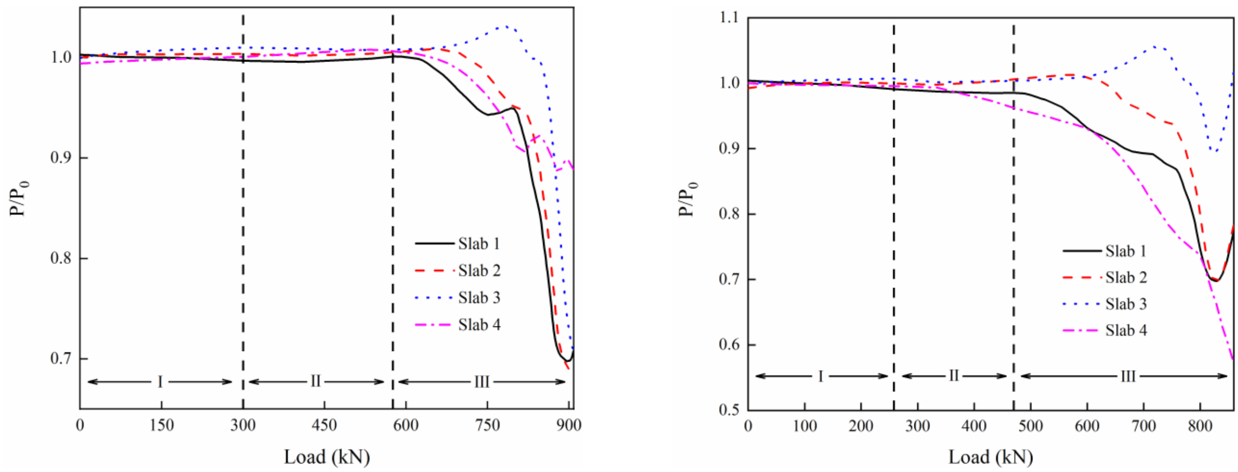

(a) CB1 (b) CB2

Fig. 11 P/P_0 -load curves

simultaneously in slab 1 and slab 2 at the load of 258 kN, and Slab 3 slipped at the load of 335 kN. Moreover, the bolts in three slabs contacted with the holes at the loads of 470 kN, 555 kN and 696 kN, respectively.

The values of F_Z/F_f were both about 1.2 when Slab 2 and Slab 3 began to slip, indicating that their shear forces exceeded the static friction forces provided by the bolt pretightening forces. This is due to the external load F/4 applied on Slab 2 and Slab 3, leading to a larger normal compressive force F_Y. As a result, F_Y of Slab 2 and Slab 3 was larger than bolt pretightening force P, which further increased the friction between the interfaces.

The friction force between interfaces of concrete and steel can be calculated according to Eq. (9), where $x = 1$ means there is a load on the concrete slab, or $x = 0$.

$$F_Z = \begin{cases} \mu P, & x = 0 \\ \mu F_Y, & x = 1 \end{cases} \tag{9}$$

The calculation results from Eq. (9) were compared with simulation results in Table 3. The maximum error is 4.5%, indicating the accuracy of Eq. (9).

In order to investigate the compressive force between interfaces only caused by bolt pretightening force, F_Y and F/4 were obtained from the numerical simulation results so P could be calculated. Fig. 11 shows the variation of P/P_0 with load of the two models respectively, where P_0 was the sum of the initial bolt pretightening forces on a single concrete slab, and P/P_0 represented the residual pretightening action of the composite beam.

The relative longitudinal slip firstly occurred at the end of the composite beam. Therefore, the pretightening force of Slab1 began to decrease at the earliest, and then the decrement developed from the end to mid-span. However, the pretightening force of Slab 4 decreased earlier than slab 3. This is because the bending deflection in mid-span of steel beam was the largest, so the small size concrete slabs were not easy to bend. Therefore, it results in a different bending curvature between steel beam and concrete slab, which leading to an uplift in mid-span and a weakening of connecting function.

Table 3 Interface friction in loading region

Specimen	Loading area	F_Z/F_f	$\mu F_Y/F_f$	Error
CB1	Slab 2	1.167	1.177	1.0%
	Slab 3	1.192	1.230	3.8%
CB2	Slab 2	0.567	0.612	4.5%
	Slab 3	0.611	0.644	3.3%

For the model CB1, when the load reached about 600 kN, the pretightening action of Slab 1 started to decrease at first. When the load reached 825 kN, P/P_0 of Slab 1 and Slab 4 reduced by about 10%, and the maximum loss of pretightening action concrete slab reached 33.2% in ultimate state.

For the model CB2, pretightening action of Slab 1 and Slab 4 started to decrease at first at the load of about 400 kN, while those of Slab 2 and Slab 3 started to decrease at the load of about 600 kN. P/P_0 of Slab 4 decreased by 20% at the load of about 730 kN and decreased by 41.9% at most in the ultimate state. This is because the shear connection degree of CB1 is 97%, which is 1.76 times of that of CB2. As the great difference of shear connection degree, the relative longitudinal slip of CB2 was greater than that of CB1 under the same load, and the loss of pretightening action was earlier than that of CB1.

Above all, the pretightening action could keep stable before the contact of bolt shank and hole, and the loss of pretightening force could be ignored in regular service stage. Although pretightening force decreased in the ultimate state, the transformation of bolt from frictional type to pressure type could still ensure the shear resistance no less than before. It can be seen that larger shear connection degree helps to reduce the longitudinal relative slip and keep the pretightening force in initial level.

4.2 Bolt connector

The shear connector was a key part in composite beam to make steel beam and concrete slab work together.

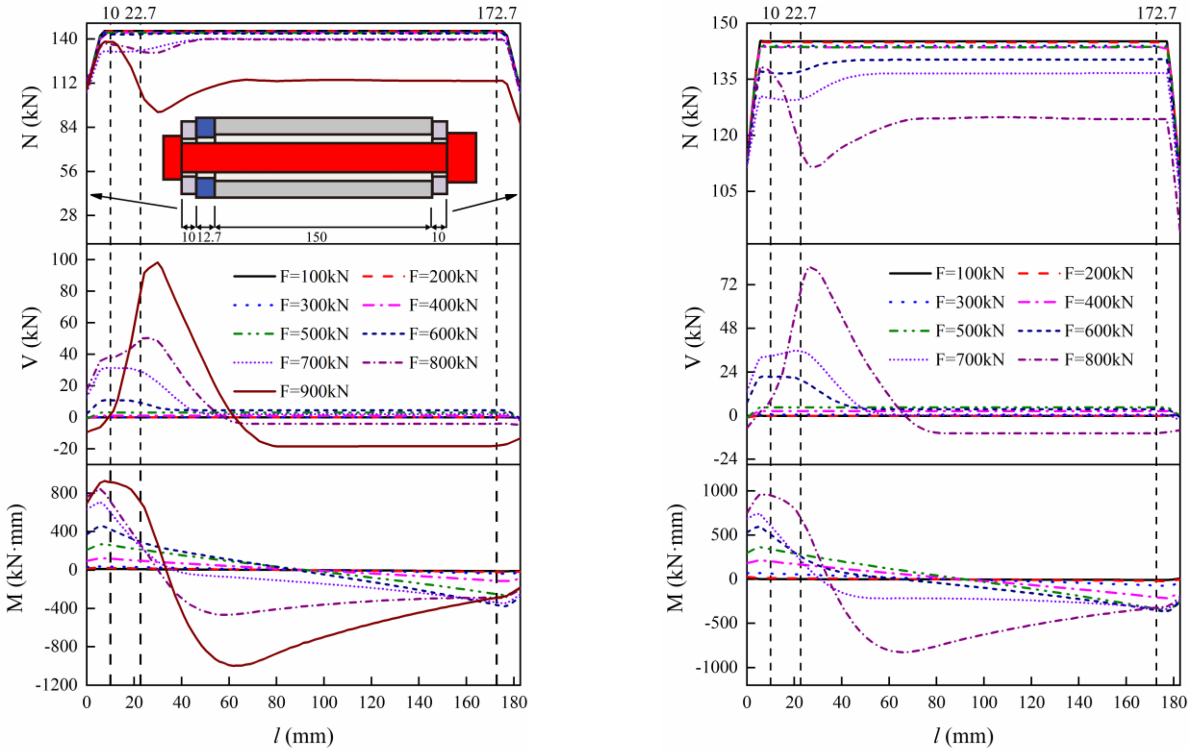

(a) CB1 (b) CB2

Fig. 12 Internal forces of the end bolt of composite beam

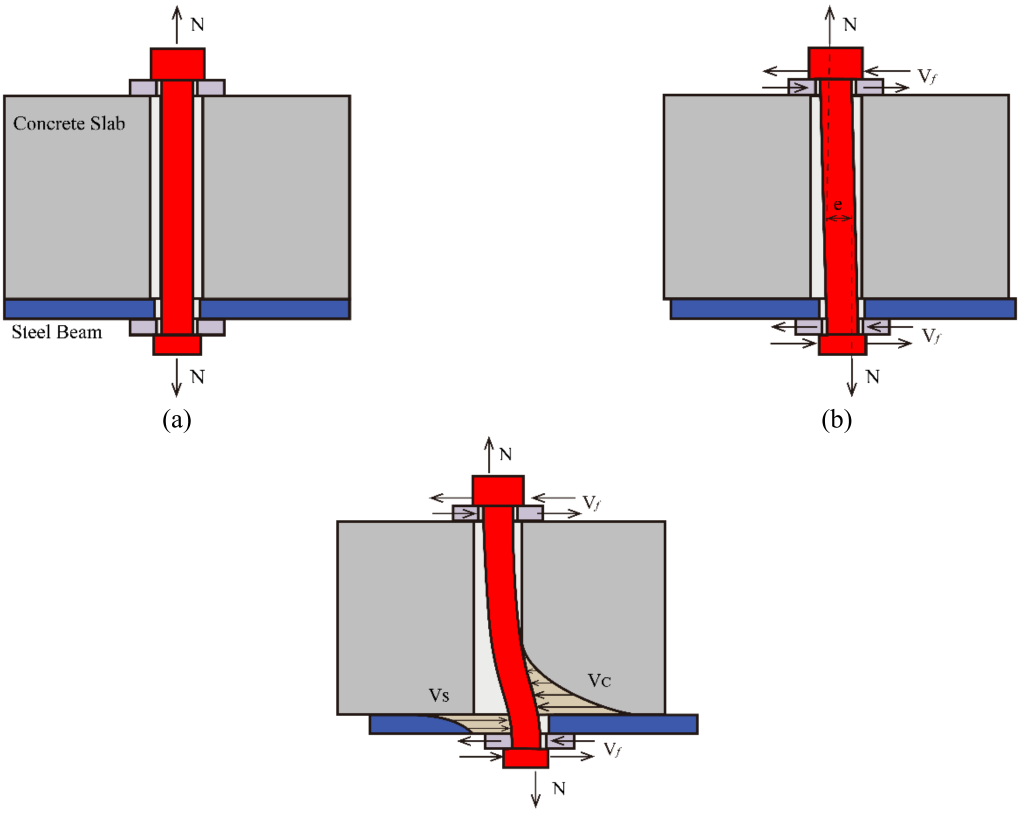

(a) (b)

(c)

Fig. 13 Mechanical mechanism of bolt

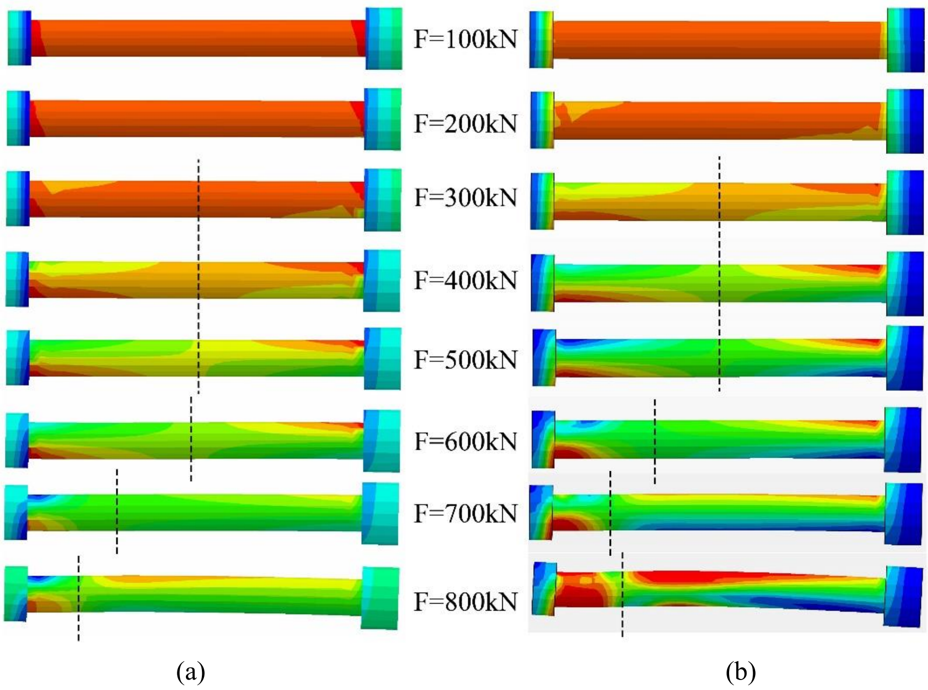

Fig. 14 The reverse bending point position of the end bolt: (a) CB1 (b) CB2

However, a connector was not in uniaxial stressed state during its service time, especially for the bolt in composite beam. Once the bolt shank contacted with bolt hole, the bolt worked as a shear member within the state of triaxial stress.

The relationship between external load and bolt internal force along the axial direction was shown in Fig. 12, where l is the length of bolt as shown in Fig. 13(a).

For the bolt at the end of CB1, when the load was below 300kN, the axial force remained constant as the initial pretightening force, while the bending moment and shear force remained always zero. The ignorable change of internal force indicated a frictional type bolt within uniaxial stressed state, as shown in Fig. 13(a). As the load reached 300~600 kN, although certain relative slip between steel beam and concrete slab was not big enough to cause the contact of bolt shank and hole, the relative motion trend between the gasket and the nut caused a tangential friction force V_f acted on bolt. In addition, the offset of the bolt lead to a eccentricity of axial force N. Under the action of eccentricity e and shear force V_f, the bolt bending moment increased continuously with the reverse bending point remained unchanged in the middle of the bolt shank, as shown in Figs. 13(b) and 14. When the load reached 700~800 kN, the internal forces of bolt changed obviously. Specifically, the axial force of bolt was greatly reduced by 51 kN, indicating a large loss of pretightening force. This was consistent with the change of F_Y demonstrated in Fig. 11. At the same time, shear deformation had occurred on account of the contact of bolt shank and hole, while the shear force maximum increased to 98 kN. The bending moment of bolt increased rapidly with the reverse bending point obviously moved to the side of the steel beam.In this stage, the bolt was subjected to axial force, shear force combined bending moment, as shown in Figa. 13(c) and 14.

It can be seen from above that the complex stress of the bolt started from the relative slip of the steel-concrete interface, and the local forces near the interface changed even greatly. Furthermore, the relationship between axial force and shear force at the position of l=24~36 mm was analyzed quantitatively, as shown in Fig. 15. Where $|\Delta N|$ was absolute value of axial force reduction, and ΔV was increment of shear force.

The relationship between axial force and shear force can be divided into five stages, in which the $\Delta V/|\Delta N|$ were 1, 2, 4, 2 and 1, respectively. The load of CB1 in Stage C was 700~800 kN, while the load of CB2 was 600~700 kN. In this stage, large shear deformation occurred due to the contact of shear shank and hole, so the shear force increased the fastest. After that, the concrete slab deformation continued to increase with the growing load, which lead to a rapid loss of pretightening force and reduction of $\Delta V/|\Delta N|$, as shown in the Stage D and Stage E of Fig. 15.

It can come to the conclusion that the bolt was in uniaxial stressed state with very small shear and bending moment in the normal service stage. In the ultimate state, the bolt was in the complex stress state. Although the combination function of concrete slab and steel beam was still good, the contact between bolt and hole should be postponed as far as possible to reduce the complex stress of bolt.

5. Parametric analysis

For assembled composite beams with no post-cast zones, the mechanical properties were well analyzed (Ataei 2016). Nevertheless, influences of the designed assembly parameters, which play vital roles in construction process,

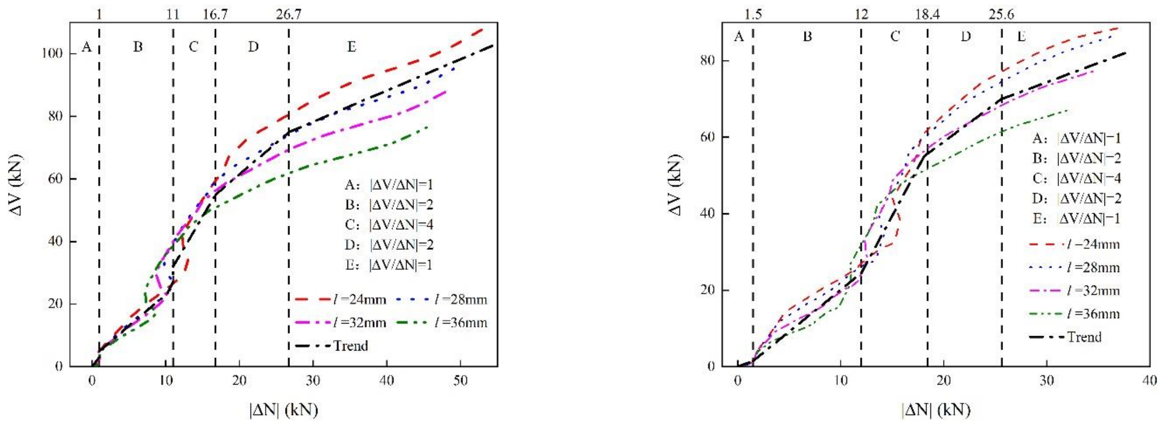

(a) CB1 (b) CB2

Fig. 15 $\Delta V - |\Delta N|$ curves

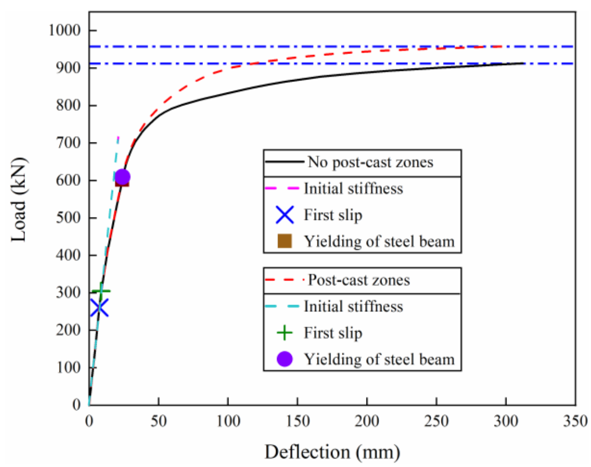

Fig. 16 Load-deflection curves of composite beam without post-cast zone

were not studied yet. In order to investigate the assembly performance of bolt connected composite beams, the influence of absence of post cast zones were compared. Besides, parametric analysis was carried out on the size and location of splicing gap. Based on this, the size of concrete slabs in the mid-span was optimized.

5.1 Influence of post-cast zones

Composite beams with no post cast zones were beneficial for assembly. However, rotation and deformation between concrete slabs may occur when the composite beam subjected to a large bending load. Therefore, the mechanical properties of composite beams with and without post-cast zones were compared and analyzed based on the model of CB1 by changing the interaction between concrete slabs. For slabs model without post-cast zones, splicing gap was ignored and slabs were not tied to each other. The load-deflection curves of them were compared in the Fig. 16. It is obvious that post cast zones had a relatively small influence on the initial stiffness, first slip load and beam yield load. What’s more, for the composite beam with and without post-cast zones, the two curves were nearly the same before the yield of steel beam, while the stiffness degradation and ultimate bearing capacity varied a lot. The ultimate bearing capacity decreased by 4.7% after removing post-cast zones, indicating a little disadvantage in the ultimate state. It was because the bottom of concrete slabs without post-cast zones cannot withstand tensile stress, so the deformation of the composite beam was increased and the compressive failure of the top slab was accelerated, as shown in Fig. 17.

In general, if the splicing gap between concrete slabs is small enough, composite beam without post-cast zones has similar behavior to the post cast one. Both of them can meet the requirement in normal service stage.

5.2 Influence of splicing gap size

For the composite beam without post-cast zone, it is inevitable that splicing gap between the concrete slabs (Δ) will exist because of the constructional and fabricated error. However, large gap has ignorable effects on the initial bending stiffness and mechanical behavior after yielding of steel beams. In this paper, influence of gaps ranges from 0 to 10 mm were studied to investigate the acceptable and reasonable splicing gaps for project.

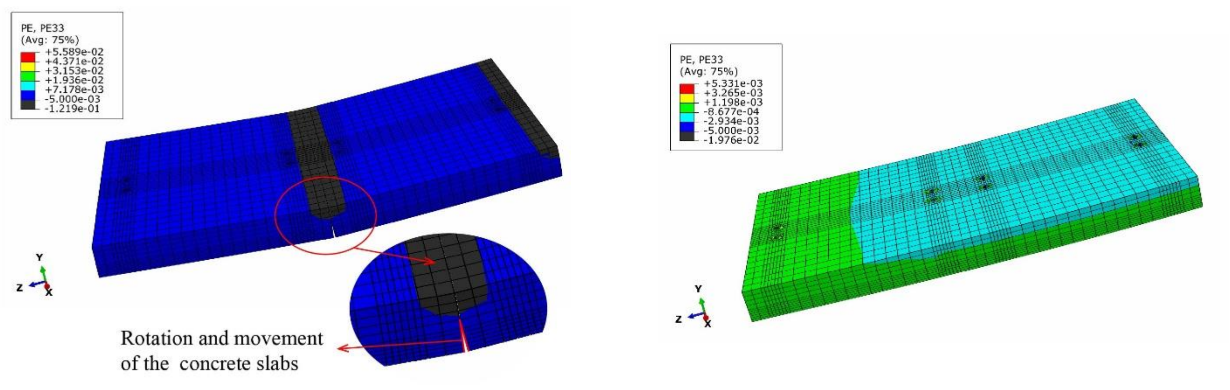

(a) Concrete slabs without post-cast zone (b) Concrete slabs with post-cast zone

Fig. 17 Z-direction Strain of concrete slabs

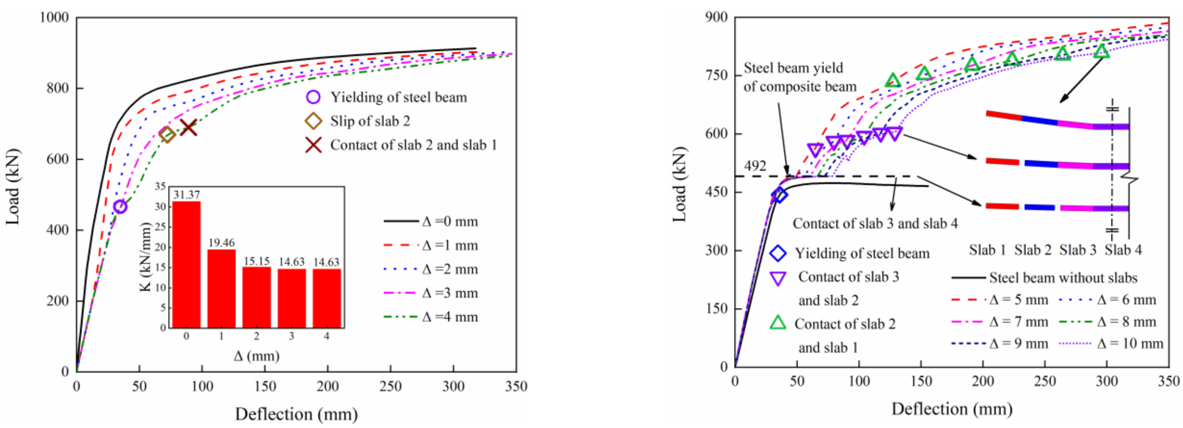

(a) Δ=0~4 mm (b) Δ=5~10 mm

Fig. 18 Load-deflection curves of composite beam

5.2.1 Influence on ultimate bearing capacity

The load-deflection curves of composite beams with different splicing gaps were shown in Fig. 18. As for the gap of 0~4 mm, there was no inflection points on the curves. That is to say, the bending curvature of beam made concrete slabs contacted each other and worked together. As for the gap of 5~10 mm, there were inflection points in the curve, indicating that it is the horizontal slippage that made concrete slabs contacted each other and worked together.

Take Δ=5 mm as an example, only Slab 4 was stressed at the beginning of loading. When the load reached 492 kN,nearly 10% larger than the yield load of pure steel beam, the bottom flange of steel beam in composite beam yielded. Furthermore, the bending stiffness decreased dramatically, and the curves' first plateau emerged. As the deflection kept growing, splicing gaps between Slab 4 and Slab 3 were eliminated, leading to a stress redistribution and stiffness recovery. In this way, the bearing capacity continued to increase until the friction of Slab 3 was overcome. Similarly, the longitudinal slippage occurred suddenly and the second plateau appeared. In this order, concrete slabs came to work together until all of them engaged in.

It can be seen from the Fig. 18 that splicing gaps have a relatively small impact on the ultimate bearing capacity. Each 1 mm increase in splicing gap led to only a 5 kN decrease in the ultimate bearing capacity for splicing gaps range from 0~4 mm, and merely a 10 kN decrease for splicing gaps range from 5~10 mm. However, its influence on the initial bending stiffness cannot be ignored. The initial tangent stiffness was calculated by the displacement value of 0.5 times the ultimate bearing capacity. Compared with composite beam with no gap, the initial bending stiffness decreased 38.0% and 51.7% when the gas was 1 mm and 2 mm, respectively. But for gaps larger than 2 mm, the initial bending stiffness did not decrease any more. That was because only Slab 4 worked at the first in the composite beam with larger gaps. The initial bending stiffness was just provided by the steel beam and Slab 4, which is only 11.38% higher than that of the bare steel beam. Moreover, the concrete slab contacted each other gradually from the mid-span to the end. When each two slabs contact, the stiffness of the composite beam will be significantly improved. With the increase of splicing gap, the contact of each two slabs required greater bending deformation.

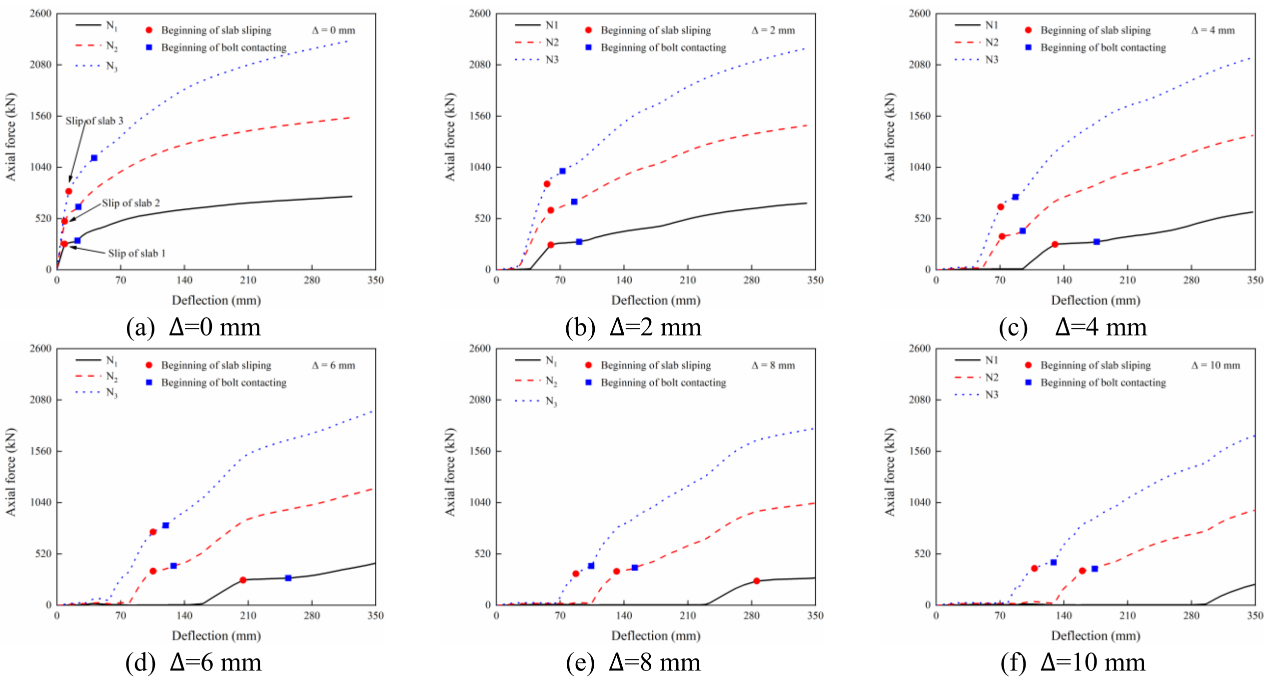

Fig. 19 N_i-deflection curves

5.2.2 Influence on pressure between concrete slabs

Concrete slabs were the main compression members in composite beams. Nevertheless, the existing splicing gaps made the slabs out of contact and weaken their effect in composite beam. In order to look into the influence on pressure between concrete slabs, analysis was carried out on composite beams with splicing gaps of 0~10 mm. As the structure is symmetrical, half model of the composite beams was established. Then contact pressure of three slabs was plotted in Fig. 19.

It can be seen from the figure that N3＞N2＞N1, that is to say, the larger bending moment at the mid-span led to a larger contact pressure. Apart from the curves in the Fig. 19(a), all of the other curves shared a horizontal plateau at the beginning. For composite beams without splicing gaps in Fig. 19(a), all the slabs worked together and cooperated with steel beam. Whereas, for those ones with splicing gaps, the deflection threshold value for activation of concrete slabs increased with the growth of gaps, as shown in Figs. 19(b)-19(d). For every 2 mm increase in splicing gap, the deflection of composite beam increased by about 50 mm when Slab1 is involved in compression. Moreover, the initiation points of slab slipping and bolt contacting were plotted in the figure. For composite beams without splicing gap, the order of concrete slabs slip was determined by the longitudinal shear force. For example, the longitudinal shear force of Slab 1 was the largest, so the friction of Slab 1 was overcome to slip firstly. For composite beams with splicing gaps, the order of concrete slabs slip was determined by the order of their participating in work. For composite beams with gaps of 0~6mm, Slab 3 and Slab 2 start to slip at the same time basically, while Slab 1 was later than them obviously. However, for composite beams with splicing gaps larger than 8mm, Slab 3 and Slab 2 cannot slip simultaneously, and the slippage occurs from Slab 3 to Slab 1 gradually.

In conclusion, the deflection of beam and bolt connectors had been extremely large before all the concrete slabs participated into work. As a result, the smaller the gap is, the more synchronously each concrete slab were stressed. To ensure the initial bending stiffness, the splicing gaps were recommended within 1 mm.

5.3 Influence of position of splicing gaps

Based on the research above, the influence of position of splicing gaps was studied in order to obtain a best installation order of concrete slabs. In different numerical models, only one gap was set in different positions for convenient.

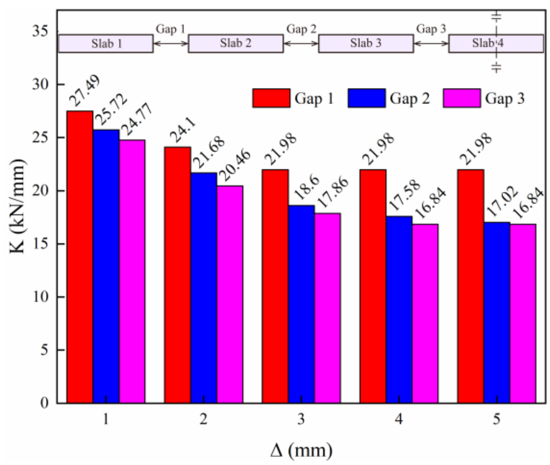

Fig. 20 Initial stiffness of composite beam with various gap sizes and positions

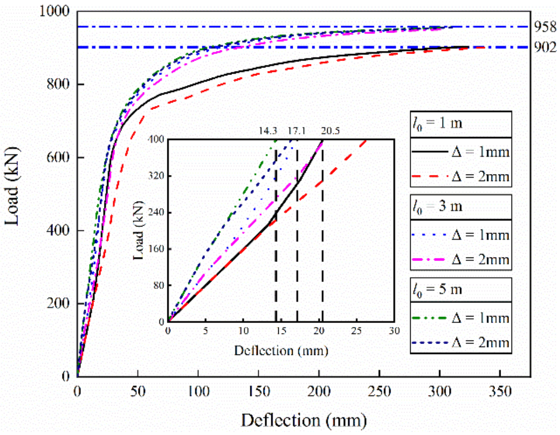

Fig. 21 Load-deflection curves with various mid-span slab sizes

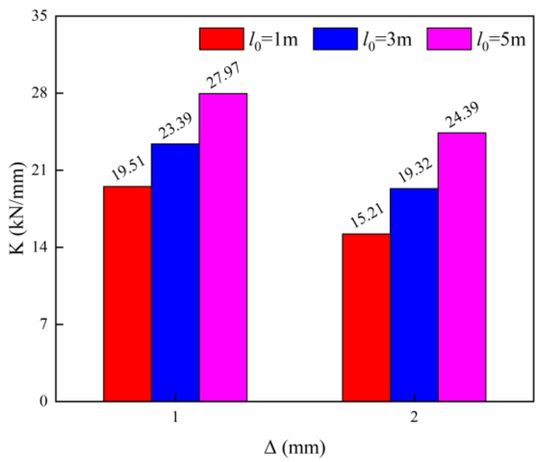

Fig. 22 Initial stiffness with various mid-span slab sizes

The initial stiffness of composite beams with gaps of various positions and sizes were demonstrated in Fig. 20. When the splicing gap was located at Gap 3, the stiffness decreased most, while the Gap 1 let to the least decrement.

This was because the bending moment at the mid-span was the largest, so the flexural capacity provided by concrete slabs accounted for a greater proportion in the composite section. Furthermore, when Δ= 1 mm , compared to Gap 1, Gap 2 and Gap 3 result in the initial stiffness reductions of 6.5% and 9.8%, respectively. When Δ= 5 mm, the reductions reached to 22.6% and 23.4%, indicating a greater position sensitivity for composite beam with larger splicing gaps. In the case of unavoidable prefabrication error, large splicing gap should be chosen to be left in the end of beam. The proper order to slab installation is from mid-span to both ends.

5.4 Optimization of concrete slab at mid-span

According to the research above, in order to ensure the stiffness of composite beams, the splicing gap must be controlled within a very small value, which greatly increased the difficulty of construction. In order to solve this problem, the size of mid-span concrete slab was improved reasonably. In the numerical model, the size of the mid-span concrete slab l_0 was changed from 1m to 3 m and 5 m respectively, while the size of the rest slabs were still 1 m. Moreover, two sizes of splicing gaps were tried between the concrete slabs.

After improving the size of the mid-span concrete slab, the influence of gap on the bearing capacity and stiffness of the composite beam was shown in Figs. 21 and 22. For composite beams with Δ of 1mm and 2mm, when l_0 increase from 1 m to 3 m, the ultimate bearing capacity increase by 5.64% and 5.40% respectively, indicating a relative small influence on strength. However, when Δ=1 mm, the initial stiffness increased by 19.95% and 43.3% as l_0 increased from 1m to 3m and 5m, respectively; when Δ=2mm, the increments were 27.0% and 60.4%. The obvious strengthen of stiffness might owe to the larger size of mid-span slab. That is to say, increasing the size of the mid-span concrete slab is equivalent to removing the most negative mid-span splicing gap. The stiffness of composite beam with l_0 of 3 m and Δ of 2 mm was equal to that with l_0 of 1m and Δ of 1 mm.

It can be concluded that the increase of l_0 can cover the stiffness reduction caused by splicing gap Δ. When the size of mid-span slab is increased to 3 m, the splicing gap can be extended to 2 mm; when the size is increased to 5 m, the splicing gap can be even larger. Therefore, in real project, the construction accuracy can be relaxed by reasonably increasing the size of mid-span concrete slabs.

6. Conclusions

Various numerical simulations have been conducted to investigate the static behavior of bolt connected concrete-steel composite beams without post-cast zone. The model was validated by test data at first. Then the size, position of splicing gap were analyzed, and the relationship between the structural behavior and the variables were verified. Stress mechanism of high strength frictional bolt in composite beam was investigated, and certain suggestion and optimization of concrete slab were proposed. Conclusions were drawn as following.

- In the normal service stage, the bolt is basically in the state of unidirectional stress with the loss of pretightening can be ignored. In the Elastic-plastic stage, the loss of pretightening can be up to 41.9%, and the bolt is in the complex stress state after turning into pressure type. Although the combination function of concrete slab and steel beam is still good, the contact between bolt and hole wall should be postponed as far as possible to reduce the tangential deformation of bolt.
- The larger shear connection degree is beneficial to maintain the pretightening, delay the contact between bolt and hole, and reduce the tangential deformation of composite beam.
- If the splicing gap between concrete slabs is small enough, the absence of post-cast zone has little influence on the initial flexural rigidity, first slip load and steel beam yield load of composite beams, which can meet the normal

service requirements. However, the ultimate bearing capacity will be reduced by 8.5% with the absence of post-cast zone.

- When the splicing gap is inevitable, the smaller the gap is, the more synchronous each concrete slab was stressed, and the smaller the initial stiffness and ultimate bearing capacity loss is. When the splicing gap is greater than 4 mm, the concrete slab contact needs greater deflection deformation of beam, and the bearing capacity curve will show discontinuous growth stage. The splicing gaps were suggested to be less than 1mm in the project to limit the initial stiffness loss within 25.6%.
- Splicing gap in mid-span make the most adverse effect on the stiffness. The gap of 1mm in the mid-span leads to a reduction in stiffness of 9.89% compared with the gap in the end of beam. It is recommended to install the concrete slabs from the middle to the end in turn, leaving a large gap at the end.
- For the mid-span slab with size larger than 3 m, the rotation and flexural deformation between two slabs could be reduced to the same level of post-casted concrete slab. As result, when the size of mid-span slab is increased to 3 m, the splicing gap can be extended to 2 mm; when the size is increased to 5 m, the splicing gap can be even larger.

Acknowledgements

The authors gratefully acknowledge the financial support from the National Natural Science Foundation of China (No. 51708384), Natural Science Foundation of Shanxi Province, (No.201801D221216 and No.201901D211017), Science and Technology Project for Oversea Scholars in Shanxi Province (No. DC1900000602), and Science & Technology Project of State Grid Shandong Electric Power Company (No. 2021A-132).

References

Ataei, A. and Zeynalian, M. (2021), "A study on structural performance of deconstructable bolted shear connectors in composite beams", *Structures*, **29,** 519-533. 10.1016/j.istruc.2020.11.065,

Ataei, A., Bradford, M.A. and Liu, X.P. (2016), "Experimental study of composite beams having a precast geopolymer concrete slab and deconstructable bolted shear connectors", *Eng. Struct.,* **114,** 1-13. 10.1016/j.engstruct.2015.10.041.

Balkos, K.D., Sjaarda, M., West, J.S. and Walbridge, S. (2019), "Static and fatigue tests of steel-precast composite beam specimens with through-bolt shear connectors", *J. Bridge Eng.*, **24**(5), 04019036. 10.1061/(ASCE)BE.1943-5592.0001382.

Chen, Y.T., Zhao, Y., West, J.S. and Walbridge, S. (2014), "Behaviour of steel–precast composite girders with through-bolt shear connectors under static loading", *J. Constr. Steel Res.*, **103**, 168-178. 10.1016/j.jcsr.2014.09.001.

Dai, X.H., Lam, D. and Saveri, E. (2015), "Effect of Concrete Strength and Stud Collar Size to Shear Capacity of Demountable Shear Connectors", *J. Struct. Eng.,* **141**(11) 04015025. 10.1061/(ASCE)ST.1943-541X.0001267.

Dallam, L.N. (1968), "Push out tests with high strength bolt shear connectors", Report for Missouri State Highway Department, Department of Civil Engineering, University of Missouri-Columbia (MI).

Fan, J.S., Gou, S.K., Ding, R., Zhan, J. and Shi, Z.J. (2020), "Experimental and analytical research on the flexural behaviour of steel–ECC composite beams under negative bending moments", *Eng. Struct.*, **210**, 110309. 10.1016/j.engstruct.2020.110309.

Han, Q.H., Xu, J., Xing, Y. and Li, Z.L. (2015), "Static push-out test on steel and recycled tire rubber-filled concrete composite beams", *Steel Compos. Struct.*, **19**(4), 843-860. https://doi.org/10.12989/scs.2015.19.4.843.

Hardjito, D, Wallah, S.E, Sumajouw, D.M.J. and Rangan, B.V. (2005), "The stress-strain behaviour of fly ash-based geopolymer concrete", In: Development in mechanics of structures and material, The Netherlands: A Balkema Publishers. 831-834.

Kwon, G., Engelhardt, M.D. and Kli1ngner, R.E. (2010), "Behavior of post-installed shear connectors under static and fatigue loading", *Steel Constr.*, **66**(4), 532-541. 10.1016/j.jcsr.2009.09.012.

Lee, J. and Fenves, G.L. (1998), "Plastic-damage model for cyclic loading of concrete structures", *J. Eng. Mech.,* **124**, 892-900. 10.1061/(ASCE)0733-9399(1998)124:8(892).

Liu, J., Ding, F.X., Liu, X.M. and Yu, Z.W. (2016), "Study on flexural capacity of simply supported steel-concrete composite beam", *Steel Compos. Struct.*, **21**(4), 829-847. https://doi.org/10.12989/scs.2016.21.4.829.

Liu, X.P., Bradford, M.A. and Ataei, A. (2017), "Flexural performance of innovative sustainable composite steel-concrete beams", *Eng. Struct.,* **130,** 282-296. 10.1016/j.engstruct.2016.10.009.

Loh, H.Y., Uy, B. and Bradford, M.A. (2006), "The effects of partial shear connection in composite flush end plate joints Part II—Analytical study and design appraisal", *J. Constr. Steel Res.*, **62**(4), 391-412.

Marshall, W.T., Nelson, H.M. and Banerjee, H.K. (1971), "An experimental study of the use of high-strength friction-grip bolts as shear connectors in composite beams", *Struct. Eng.*, **49**, 171-178.

Nie, J.G., Tang, L. and Cai, C.S. (2009), "Performance of Steel-Concrete Composite Beams under Combined Bending and Torsion", *J. Struct. Eng.,* **135**, 1048-1057. 10.1061/ASCEST.1943-541X.0000042

Pathirana, S.W., Uy, B., Mirza, O. and Zhu, X.Q. (2016), "Flexural behaviour of composite steel–concrete beams utilising blind bolt shear connectors", *Eng. Struct.,* **114**, 181–194 10.1016/j.engstruct.2016.01.057.

Pavlović, M., Marković, Z., Veljković, M. and Buđevac, D. (2013), "Bolted shear connectors vs. headed studs behaviour in push-out tests", *J. Constr. Steel Res.*, **88**(9), 134-149. 10.1016/j.jcsr.2013.05.003.

Rehman, N., Lam, D., Dai, X. and Ashour, A.F. (2016), "Experimental study on demountable shear connectors in composite slabs with profiled decking", *J. Constr. Steel Res.*, **122**, 178-189. 10.1016/j.jcsr.2016.03.021.

Sheehan, T., Dai, X.H. and Lam, D. (2018), "Flexural behaviour of asymmetric composite beam with low degree of shear connection", *J. Constr. Steel Res.*, **141**, 251-261. 10.1016/j.jcsr.2017.11.018.

Shi, G., Shi, Y.J., Wang, Y.Q. and Bradford, M.A. (2008), "Numerical simulation of steel pretensioned bolted end-plate connections of different types and details", *Eng. Struct.*, **30,** 2677-2686. 10.1016/j.engstruct.2008.02.013.

Suwaed A.S.H. and Suwaed Karavasilis, T.L. (2018), "Removable shear connector for steel-concrete composite bridges", *Steel Compos. Struct.*, **29**(1), 107-123. https://doi.org/10.12989/scs.2018.29.1.107

Tan E. L., Varsani H., and Liao F. Y. (2019), "Experimental study on demountable steel-concrete connectors subjected to combined shear and tension" *Eng. Struct.,* **183** 110–123. 10.1016/j.engstruct.2018.12.088.

Wang, Y.H., Yu, J., Liu, J.P. and Chen, Y.F. (2019), "Shear behavior of shear stud groups in precast concrete decks", *Eng. Struct*., **187**, 73-84. 10.1016/j.engstruct.2019.02.002.

Yang, T., Liu, S.Y., Qin, B.X. and Liu, Y.Q. (2020), "Experimental study on multi-bolt shear connectors of prefabricated steel-concrete composite beams", *J. Constr. Steel Res.*, **173**, 106260. 10.1016/j.jcsr.2020.106260.

Zhang, Y.J., Chen, B.C., Liu, A.R., Pi, Y. L., Zhang, J.P., Wang, Y. and Zhong, L.C. (2019), "Experimental study on shear behavior of high strength bolt connection in prefabricated steel-concrete composite beam", *Compos. Part B-Eng.*, **159**, 481-489. 10.1016/j.compositesb.2018.10.007.

Zhao, W., Lu, S.Q. and Jing, X.Y. (2020), "Shear performance of high-strength bolt connector considering different pad and bolt hole", *Structures,* **28**, 1291-1300. 10.1016/j.istruc.2020.09.050.

CC